somalogic

Discover more with the world's largest proteomic platform

350% larger menu than other platforms

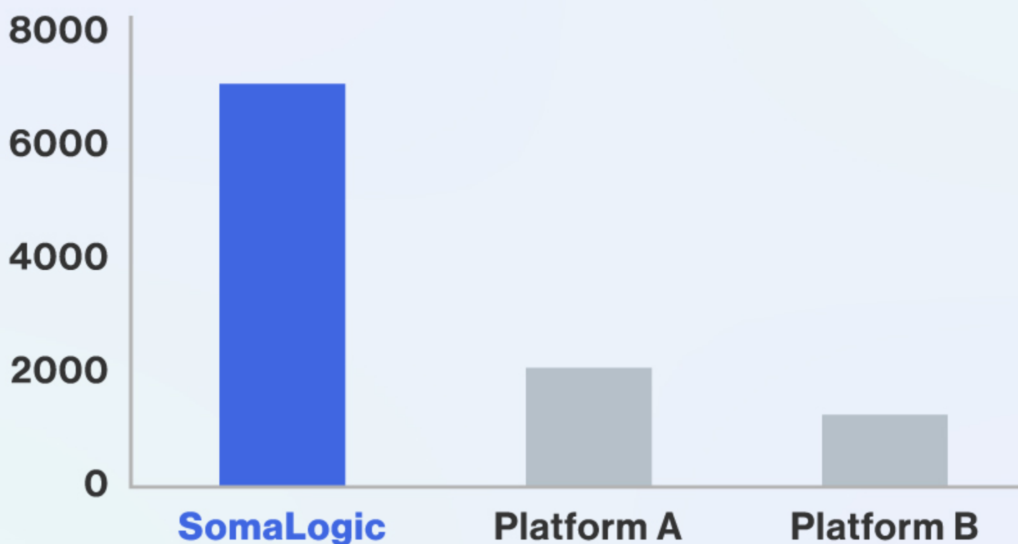

Check for updates

Received: 25 February 2021 | Revised: 22 May 2021 | Accepted: 24 May 2021
DOI: 10.1002/jms.4771

RESEARCH ARTICLE

Journal of MASS SPECTROMETRY WILEY

Application of 7N In as secondary cathode for the direct current-glow discharge mass spectrometry analysis of solid, fused high-purity quartz

Jochen Busam[1] | Gaute Stokkan[2] | Astrid Marie F. Muggerud[3] | Marisa Di Sabatino[1]

[1]Department of Materials Science and Engineering, Norwegian University of Science and Technology (NTNU), Trondheim, Norway
[2]SINTEF Industry, Trondheim, Norway
[3]The Quartz Corp, Drag, Norway

Correspondence
Jochen Busam, Department of Materials Science and Engineering, Norwegian University of Science and Technology (NTNU), Alfred Getz vei 2, 7491 Trondheim, Norway.
Email: jochen.busam@ntnu.no

Funding information
Research Council of Norway, Grant/Award Number: 268027

Abstract

Direct current glow discharge mass spectrometry with an indium-based secondary cathode technique is used to analyze solid, nonconducting, fused high-purity quartz regarding metallic impurities of relevance to the solar industry. Details of the analytical routines are presented. In this work, the secondary cathode design and glow discharge conditions are optimized beyond the commonly applied practices. In addition, relative sensitivity factors (RSFs) for these optimized conditions are established and compared to previously published results. The results indicate that the technique enables stable measurements with detection limits down to the part per billion (ppb) range.

KEYWORDS
direct current glow discharge mass spectrometry, indium, quartz, secondary cathode, silica

1 | INTRODUCTION

Glow discharge mass spectrometry (GDMS) is one of the industry standards for the analysis of trace elements in conducting, solid samples.[1,2] It readily offers detection limits in the part per billion (ppb) range and below, a high sample throughput and simple sample handling.[3,4] Its high 1-D resolution makes it also suitable for depth profiling.[5,6] One application field is the photovoltaic industry where GDMS offers ultra-trace level detection limits of transition elements in semiconductors such as silicon.[2,7,8]

A common setup is the direct current direct current (dc)-GDMS, where, under low gas pressure, a voltage is applied between a pin-shaped or flat sample and a discharge cell, creating a glow discharge plasma in the cavity of the cell. The conducting sample acts as cathode attracting the plasma ions, which in turn sputter the sample, while the cell acts as anode through which ions are extracted into the mass spectrometer. In the flat setup, the sample holder acts as insulator and part of the anode.[4,7]

GDMS offers a major advantage over the more commonly used inductively coupled plasma inductively coupled plasma mass spectrometry (ICP-MS) regarding the analysis of refractory and inert materials. Although ICP-MS requires tedious digestion steps, GDMS offers the ability to analyze them directly.[7,9] However, as these samples are often nonconducting, dc-GDMS requires a modification to be applicable. There are two common approaches to this modification. Powdered samples are mixed with a conducting host material and pressed into pin or pellet shape.[10–12] For solid samples, the secondary cathode method is applied. Here, a mask made of a conductive material is placed on the flat sample, which is exposed to the GD through typically a round aperture in the mask.[13] This technique has been demonstrated for a range of different samples whereby tantalum as mask material produced the best results.[11–18] Indium as secondary cathode applied through a coating process onto a soda-lime glass pin sample has been

This is an open access article under the terms of the Creative Commons Attribution License, which permits use, distribution and reproduction in any medium, provided the original work is properly cited.
© 2021 The Authors. *Journal of Mass Spectrometry* published by John Wiley & Sons Ltd.

demonstrated,[19] and the use of indium as directly applied mask material has been introduced by the manufacturer of the Astrum GDMS, Nu instruments.[20] Most recently, the technique has been demonstrated in an application note for yttrium and zirconium containing ceramics.[21]

In the present work, we optimize the dc-GDMS secondary cathode technique with an indium mask for flat fused quartz (also called silica) samples in regard to mask design and discharge conditions in order to improve quantification and limits of detection (LODs). The selection of analyzed impurities is made based on their importance and detrimental effects during the solar cell production.

1.1 | The secondary cathode method

Here, the conducting mask material is sputtered and redeposited on the nonconducting sample. This allows the sample to also attract plasma ions and consequently be sputtered. The redeposition strongly depends on the discharge pressure, which in turn dictates current and voltage conditions. Optimal conditions can be matrix dependent, as too high pressure will lead to complete coating of the sample while too low pressure causes an unstable discharge.[14,15]

A high purity mask material and a high ratio of matrix to mask signal are preferred and important to reduce contributions of any impurity from the mask to a background signal.

Altering the discharge conditions can allow to optimize the signal intensity and matrix to mask ratios.[15] A high signal and an optimal ratio are crucial for the performance of the analysis in regard to detection capabilities. The optimal discharge conditions for the secondary cathode technique may therefore lie in a regime where the quantification is sensitive to variations in the discharge conditions.[22]

1.2 | Secondary cathode material

For this work, indium was chosen as it is available in high purities of up to 7N. Indium was previously omitted for its softness and low melting point, causing a short circuit in the discharge setup.[14] The softness and low melting point of indium were not found to be an issue during this study. Presumably, this is due to the low temperature of the sample, as the discharge cell is cooled by liquid nitrogen and the power input at the chosen discharge settings is low compared to standard settings.

Besides being pure, the mask material should also produce a high matrix to mask signal ratio. This should require a material with a low sputtering yield.[14] This is a possible disadvantage of indium as it has a high sputtering yield compared to tantalum and SiO_2. The sputtering yield ratios are approximately SiO_2:Ta 1:1 and SiO_2:In 1:4.[23–26] It was found for round aperture aluminum and silver secondary cathodes, which have a lower sputtering yield then indium, that either it was not possible to establish a stable discharge or it resulted in complete coating of the sample by mask material.[14,15,25] When indium is used as round aperture secondary cathode the situation could be similar or worse as indium has a higher sputtering yield than aluminum or silver.

1.3 | Secondary cathode geometry

The anode opening diameter (the front tantalum aperture of a flat sample holder) and cathode opening diameter (round aperture mask) influence the discharge conditions and thus matrix to mask ratio and signal intensity.[14,15] Milton and Hutton[14] found for tantalum an optimum anode diameter of 5 mm and cathode diameter of 4 mm, resulting in a 1:6 matrix to mask signal ratio, whereas the best achievable ratio with an anode diameter of 10 mm and a cathode diameter of 6 mm was 1:33. The thickness of the mask should be as small as possible for an optimal signal intensity and ratio, while still being thick enough to sustain reasonable run times.[27] For indium, it is common to use masks with several slit openings,[20,21] whereby narrow slits are chosen when an even sputtering is desirable and wider slits possibly improve the signal intensity and ratios.

1.4 | Quantification and RSF

The quantification in GDMS is enabled by the so-called relative sensitivity factors (RSFs). They account for the different factors that influence the measured ion intensity of an element. The concentration $C_{X/M}$ of element X contained in a sample matrix M is given by Equation (1), where I_x and I_M denote the measured, abundance corrected ion beam intensities.

$$C_{X/M} = \frac{RSF_X}{RSF_M} \times \frac{I_X}{I_M}. \quad (1)$$

The dominant factors influencing RSFs are transport and ionization processes in the plasma. In the latter, electron impact ionization is considered of minor importance, and Penning ionization unselective for most elements, while asymmetric charge transfer ionization is responsible for large variations of RSFs for some elements depending on their electron configuration.[28–30]

Normally, the effects of different matrices are small and the element specific RSFs stable so that tables with "standard" RSFs were established and can be applied for most conductive matrices and between similar GDMS instruments under similar operating conditions.[28,31]

However, there are in practice many experimental factors that can influence the RSFs:

- Discharge conditions, characterized by current, voltage, and gas flow/pressure, influence quantification.[22,32–34]

This is especially relevant for the secondary cathode method as it may require nonstandard discharge conditions to achieve a stable discharge with optimal signal intensity and optimal matrix to mask signal

ratio.[14–18] The optimal conditions can vary with sample and mask material and even with sample material when a similar mask is used.[17] In turn, it was found that host matrix and secondary cathode method can show the same RSFs even for different sample materials given similar masks and conditions.[11]

- Pin and flat samples show differences that can be explained by a mix of ionization processes.[11,35]
- For semiconducting and nonconducting samples, contrary to conducting samples, matrix specific RSFs might be required to achieve precise quantification.[12,34]
- Temperature influences quantification.[11,36] Despite liquid nitrogen cooling, a variation in sample temperature has been noticed qualitatively by the authors for the application of high power in the Astrum.

1.5 | Clusters

Schelles and Van Grieken[17] and Tong and Harrison[10] demonstrated that during GDMS analysis of oxide materials, a significant amount of matrix material can be present in the plasma as clusters, especially as diatomic molecules of the form MO+ (where M denotes any element) and their relative abundance correlates well with the bond strength among the atoms. It was found by Schelles and Van Grieken[17] and Tong and Harrison[10] and also verified in this work that oxide molecules with a lower bond strength than SiO+ are only present in low quantities. This is the case for the transition metals measured in this work[37]; hence, their effect can probably be safely neglected in regard to the overall error of the measurement.

2 | EXPERIMENT

2.1 | Instrumentation

This work was performed with a Astrum (Nu Instruments), a double focusing low-flow dc-GDMS which is similar to the VG9000 (Thermo Scientific) used in many previous publications.[7] More details on the Astrum, respectively the VG9000, can be found elsewhere.[7,22,31]

The experiments were conducted using a flat cell with a front anode plate opening of 10 mm. During the measurement of pure conducting samples, aluminum signals typically stayed above 30 ppb though the aluminum levels in the samples were known to be lower. A standard assembly of Astrum''s flat cell is supplied with Al2O3 insulators. They were identified as a source of the aluminum contamination and replaced by custom-made SiO_2 insulators. By that the aluminum levels were reduced significantly and the levels for other elements were not altered.

Craters profiles were acquired with a MarSurf M 400 at 2000 points per mm. During the measurements, the instrument was unstable which resulted in strong noise. The profiles where therefore smoothed with a moving average window of 20.

2.2 | Sample preparation

A fused quartz glass sample was polished in several steps using fixed abrasive diamond disks and water down to 1-μm grit size. No liquid abrasive mixtures were used to prevent contamination. A fine polished sample surface is crucial because it reduces surface and subsurface damage such as microcracks that can harbor contamination.[38–40] Also, the sample surface roughness influences the discharge conditions; thus, to get constant conditions, the sample should be polished in a reproducible way.[16]

The indium mask is prepared from high purity 7N indium shots provided by RASA Industries. The shots are pressed flat in-between two polytetrafluoroethylene (PTFE) sheets to a thickness of 0.2 mm. The PTFE sheets provide a clean and smooth surface to prevent structuring or contamination of the indium surface. The mask openings are cut into the flat indium pieces with a ZrO_2 blade stamp, shown in Figure 1, to provide reproducible dimensions and prevent contamination by iron.

The masks are etched for 1 min in concentrated 65% HNO_3 to remove surface contamination and possible oxide layers. Thereafter the masks are rinsed with DI water and ethanol and air dried.

2.3 | Methodology

All reported concentrations are determine using the standard RSFs supplied with the instrument, which are based on the RSFs provided by Vieth and Huneke.[28] These RSFs were acquired with conducting pin samples at discharge conditions of 3 mA and 1 kV. Thus, they might deviate from the correct values for the here presented measurements. Indium blank samples were measured under standard conditions of constant current 2 mA and voltage 1 kV. The indium masks were measured by placing them on a flat indium piece. During the measurement of quartz, the instrument was run at constant current mode with following discharge conditions: current 0.3 mA, voltage 1.5 kV, argon flow 0.17 sccm, and pressure 4.9×10^{-5} mbar in the source chamber if not stated otherwise. The samples were

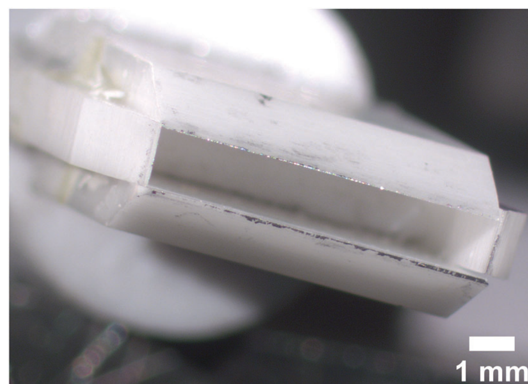

FIGURE 1 Cutting tool made from ZrO_2 blades

pre-sputtered for approximately 30 min to reach stable values. Simultaneously, the instrument parameters were tuned to optimize signal intensity and shape.

Mass spectra were acquired six times at 80 ms with the Faraday cup and at 320 ms with the ion counter for elements of low concentration. The total acquisition time was approximately 10 min. The measured concentrations were corrected for the signal contribution from contamination contained in the indium mask shown in Table 1. To account for incomplete dissociation of the silicon matrix (SiO+ clusters) the silicon signal was increased by 9.6%. The silicon signal was divided by a stoichiometric factor based on the atomic weight ratio Si/(Si+2O) = 0.47. This stoichiometric correction is the standard method by the instrument manufacturer for oxide samples.

The LOD is calculated as suggested by Milton and Hutton.[14] The background (BG) is the sum of the signal contribution from impurities in the mask and the instrument noise:

$$\mathrm{BG} = \text{mask signal} + \text{instrument noise}$$

The standard deviation σ for the background calculates from that as:

$$\sigma(\mathrm{BG}) = \sqrt{\sigma(\text{mask signal})^2 + \sigma(\text{instrument noise})^2}$$

Finally the LOD is defined as three times the standard deviation of the background:

$$\mathrm{LOD} = 3 \cdot \sigma(\mathrm{BG})$$

3 | RESULTS AND DISCUSSION

3.1 | Contamination in the indium mask

The main contaminants present in the indium mask are the most common metals aluminum and iron.[41] They are most likely introduced during the etching process because those metals are present in other experiments conducted in the same laboratory. As shown in Table 1, for those two elements, the contamination is higher than the certified indium values provided by the manufacturer. For other elements, the contamination is in part significantly lower than the certified values.

TABLE 1 Typical contamination levels (ppb) in the indium mask and certified values

Element	Average	SD	RSD%	Certified
Al	17.7	0.59	3.4	<5
Ti	0.645	0.056	8.6	<1
Cr	0.221	0.028	13	<2
Mn	0.056	0.009	16	<3
Fe	4.29	0.48	11	<1

The measured concentrations of contaminants in indium can reach high stable values over more than an hour of sputtering suggesting that they are not limited to the indium surface. With such high contamination, typically several different contaminates are present but high contamination by a single element has also been observed. Stable levels are typically obtained after 20–30 min of sputtering, whereby lower contamination levels stabilize quicker.

Flat indium pieces and masks prepared in the same batch show the same contamination as indicated in Figure 2. There is no additional contamination due to mask cutting. The consistency within a batch allows to measure one flat piece and use it as reference value for the masks prepared in the same batch, because measuring a mask and subsequently placing it on the sample can be impossible as the mask tends to stick to the underlying indium.

3.2 | Mask design, discharge conditions, and signal ratios

The typical mask design of a round aperture was explored for varying aperture diameters (from 4 to 8 mm) and discharge conditions but led only to complete coating of the exposed quartz or unstable discharge. The same was found for a design with three small holes with 2-mm diameter.

The mask design that was provided by the instrument manufacturer is shown in Figure 3A) and consists of several slits in the flat indium piece that provide narrow openings through which the sample is exposed to the GD. This allows for a stable discharge under standard or near standard conditions and uniform sputtering but was found to result in unfavorable silicon to indium signal ratios and low intensities when used with fused quartz. With this design, the crater shape is dominated by the so-called crater edge effect[42] due to the narrow slit opening resulting in deep but very narrow craters.

Outgoing from the narrow slit design, in an attempt to increase the exposed area, several designs with wider openings have been explored including four and two openings. The best design was found to be three wide slits with width of 1.3 mm and length of 6 and 7 mm

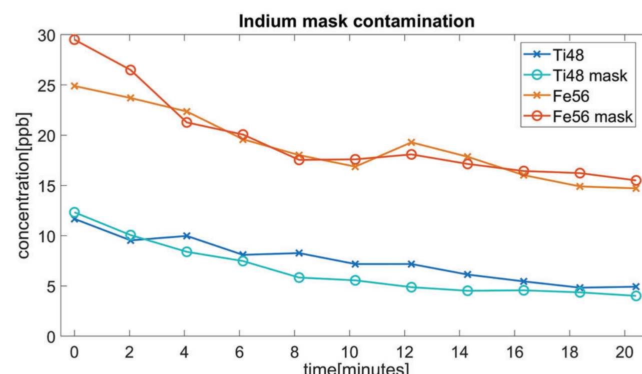

FIGURE 2 Example of high iron and titanium contamination over time in an indium mask and a flat indium piece of the same batch

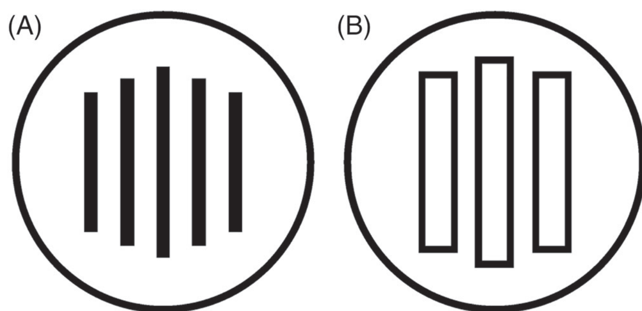

FIGURE 3 Sketch of (A) narrow slit mask design and (B) wide slit mask design

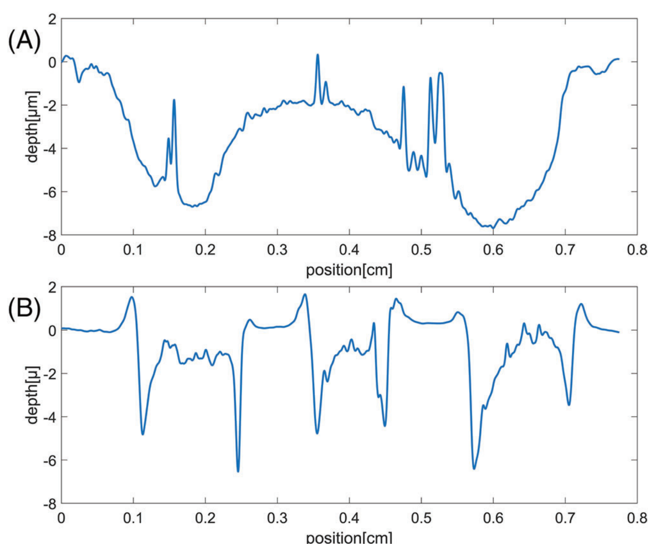

FIGURE 4 (A) Crater profile along the central window and (B) profile centrally across the three window

shown schematically in Figure 3B). This design has an exposed sample area of 0.25 cm^2, while the exposed indium area is 0.39 cm^2 (crater diameter ~9 mm) yielding an area ratio of 1:1.5.

The standard discharge conditions were unstable when using this design. The optimal conditions were found to be 0.3 mA and 1.5 kV with silicon to indium signal ratio of up to 1:35 and a stable discharge over more than 1.5 h. The signal intensity in abundance corrected counts per second (cps) were Si28 8×10^8 cps and In115 3×10^{10} cps. Typical intensity values under standard conditions are Si28 7×10^9 cps for solar grade silicon and In115 1.5×10^{11} cps for pure indium. Considering that a 4.4 times lower discharge power is used and that the exposed sample area was reduced by 60% when compared to the standard experimental setup for silicon, this mask design yields high silicon signal intensities.

As discussed previously, the anode diameter influences the discharge conditions and thus matrix to mask ratios and signal intensity. In this experiment, a 10-mm anode was used. In the literature, the best results were obtained with <10-mm anode diameters.[14,15] To further improve this method, a smaller anode diameter should be explored.

3.3 | Stability of the discharge

In the range of typical GDMS discharge conditions, the sputtering yield and signal intensity increase with current and voltage.[22,43] A higher signal intensity is desirable to improve the detection limit. In the application of the secondary cathode technique for non-conducting samples, a higher signal intensity can be hindered by unfavorable matrix to mask ratios but most commonly the loss of discharge stability is the limiting factor for signal intensity. Indeed, during the experiments using the modified mask, stable discharge was found to be limited to levels below a maximum voltage or current or power.

A two-slit mask with slits wider than 1.3 mm and smaller exposed total sample area did not yield in stable discharge conditions. This indicates that there needs to be a certain vicinity of the conductive mask to any point on the non-conductive sample to allow a stable discharge.

3.4 | Crater profiles

Figure 4 shows the crater in the quartz sample after the use of a three-window mask and ~2 h of sputtering. The spikes in the graph (e.g., Figure 4A at 0.5 cm) could not be directly associated with any physical features observed under the microscope. They might stem from contact between the profilometer tip and particles inside the crater.

Along the slit, shown in Figure 4A), the crater profile resembles the convex crater shape that is expected for conductive samples and discharge settings with a low current/high voltage.[5,43] This indicates that the overall shape of the glow discharge above the secondary cathode and nonconductive sample is similar to that of a conductive sample. Noticeable are the relatively wide crater edges. The asymmetry in the crater stems from variations in the mask position. Across the windows, shown in Figure 4B), the craters are characterized by very deep crater edges, possibly a result of the smaller crater dimension.

3.5 | Clusters

For SiO+/Si+ the amount of SiO+ clusters was found to be 9.6% ± 2%, which deviates from the 3% reported by Schelles for a macor sample (21.5% Si and 45.3% O) and discharge conditions of 0.6 mA and 1.2 kV.[17]

To correct for the presence of SiO+ and therefore incomplete dissociation of the silicon matrix, during quantification, the silicon signal is increased by 9.6%.

3.6 | Quantification

The measured concentrations at 1.5 kV are shown in Table 2 together with the percent of indium blank correction. The magnitude of relative standard deviations (RSDs) is reasonable regarding detection limits and interferences. For iron, the measured concentration has a RSD of 33% and blank of 60%, which suggests a high inaccuracy and might be reason to discard it. As the iron concentration is crucial for subsequent RSF comparison, the value is anyhow considered in the further analysis.

An example for the reproducibility of two experiments carried out in different weeks is shown in Table 3. The measurements were taken on the same sample that was repolished in between. The indium masks were from different batches, and similar discharge conditions were applied. For one of the batches, no pure indium measurement was conducted, and thus, no blank subtraction could be applied.

Therefore, only the elements with low blank are compared. The deviation lies within the margin of error of the measurements. This shows a high robustness of the method when sufficient precautions are taken regarding contamination and similar discharge conditions.

TABLE 2 Measured concentrations (ppb) at 1.5 kV and blank contribution

Element	Average	SD	RSD%	Blank%
Al	25,700	2600	10	10.3
Ti	941	70	7.4	10.3
Cr	28.7	8.5	30	35
Mn	21.7	5.2	24	19
Fe	224	74	33	60

TABLE 3 Deviation of two concentrations measurements performed in different weeks on a repolished sample

Element	Deviation%
Al	12
Ti	11
Mn	17

3.7 | RSF values

From the measured concentrations and given reference values for the fused quartz sample, the RSF values are calculated following Equation (1). The RSFs relative to $RSF_{Si} = 1$ are given in Table 4 and compared to values from the literature (the values from Vieth and Huneke[28] were relatively adjusted to $RSF_{Si} = 1$). Milton and Hutton, Schelles and Van Grieken, and Qian et al.[14,17,19] are based on glass materials with SiO_2 as primary constituent. The discharge conditions vary as Milton and Hutton[14] used 2 mA, 1000 V; Schelles and Van Grieken[17] used 0.6 mA, 1200 V and Qian et al.[19] used 1.5 mA, 2000 V on a pin sample. Among the measured RSFs and the literature values, and among the literature values themselves lies a high variation but that can be expected due to the variation in discharge conditions. Noticeable is the good agreement of aluminum with Schelles and Van Grieken[17] considering the somewhat similar discharge conditions. Compared to the work by Milton and Hutton,[14] which offers the most comprehensive set of RSFs on SiO_2-based materials, the measured RSFs are within a factor of 2, which is again reasonable regarding the difference in discharge conditions.

Outgoing from the previous table, Table 5 shows the RSFs relative to $RSF_{Fe} = 1$ compared to literature values (the values from Milton and Hutton[14] were relatively adjusted to $RSF_{Fe} = 1$).

Though iron has a high blank, which could prevent a reliable measurement, the relative RSF values are reasonable. If the

TABLE 4 Total RSF relative to $RSF_{Si} = 1$

Element	Measured	Milton and Hutton[14]	Schelles and Van Grieken[17]	Qian et al.[19]	Vieth and Huneke[28]
Al	0.359	0.621	0.3	0.84	0.709
Ti	0.296	0.245			0.214
Cr	0.794				1.14
Mn	1.04	0.878			0.755
Fe	0.387	0.590		5.09	0.510

TABLE 5 Total RSF relative to $RSF_{Fe} = 1$

Element	Measured	Milton and Hutton[14]	De Gendt et al.[11]	Schelles and Van Grieken[18]	Barnhart et al.[20]	Vieth and Huneke[28]
Al	0.928	1.05	1.45	1.4	1.43	1.39
Si	2.59	1.69	1.28	2		1.96
Ti	0.766	0.415	0.82		0.421	0.42
Cr	2.05				2.14	2.23
Mn	2.70	1.49	1.05		1.46	1.48

TABLE 6 Limits of detection (ppb) based on indium contaminants and instrument background

Isotope	Measured	Certified
Al27	71	60
Ti48	6.7	12
Cr52	27	24
Mn55	1.8	36
Fe56	58	12

measured iron concentration was far off, all the other RSFs relative to iron would be shifted either up or down. That is not the case, as they are above and below the values from other sources. The measured RSFs are again within a factor of 2 of the reference values by Milton and Hutton[14] and Vieth and Huneke[28] demonstrating that the deviations due to different discharge conditions are present but not to a severe scale.

3.8 | Limits of detection

The measured limits are based on the indium measurement used for blank subtraction shown in Table 1 considering a matrix to mask ratio of 1:35. For the certified values, an RSD of 10% has been assumed. The LODs, shown in Table 6, are comparable to or lower than the ones reported in literature for tantalum masks.[14]

The dominant limiting factor for all isotopes except Mn55 is the contribution from the mask compared to the instrument background. A reduction of indium mask contamination during sample preparation and a better matrix to mask ratio is therefore key to possible improvements of this method.

4 | CONCLUSION

For an indium secondary cathode used to analyze low-level impurities in bulk SiO_2 (silica, quartz), the optimized multi slit mask design is superior to designs with round opening or several narrow slits. Together with nonstandard discharge conditions, it makes indium well suited as secondary cathode material for the GDMS analysis of high-purity quartz. It can be an alternative to tantalum, especially if tantalum suffers from certain impurities or when tantalum itself should be quantified. The RSFs lie within a factor of 2 of previously reported values, which is reasonable regarding the difference in discharge conditions. For quartz, the discharge conditions are possibly limited and specifically dependent on the physical sample properties.

Ultimately, dc-GDMS with the indium-based secondary cathode technique proves to be a sound alternative for the analysis of solid, fused high-purity quartz without the need for hazardous chemicals and extensive sample preparation.

ACKNOWLEDGEMENTS

This work was performed in the frame of a project titled "Crucibles for next generation high quality silicon solar cells (CruGenSi)", project no. 268027, funded by the Research Council of Norway and industry partners.

ORCID

Jochen Busam https://orcid.org/0000-0002-9137-1813

REFERENCES

1. Bogaerts A, Gijbels R. New developments and applications in GDMS. *Fresenius J Anal Chem*. Jul. 1999;364(5):367-375.
2. Hoffmann V, Kasik M, Robinson PK, Venzago C. Glow discharge mass spectrometry. *Anal Bioanal Chem*. 2005;381(1):173-188.
3. Pisonero J, Fernández B, Günther D. Critical revision of GD-MS, LA-ICP-MS and SIMS as inorganic mass spectrometric techniques for direct solid analysis. *J Anal At Spectrom*. 2009;24(9):1145-1160.
4. Harrison WW, Yang C, Oxley E. Mass spectrometry of glow discharges. In: *Glow Discharge Plasmas in Analytical Spectroscopy*. John Wiley & Sons, Ltd; 2003:71-96.
5. Raith A, Hutton RC, Huneke JC. Optimization of quantitative depth profiling with glow discharge mass spectrometry. Part 1. Optimization studies on crater shape and time-depth conversion. *J Anal At Spectrom*. 1993;8(6):867-873.
6. Di Sabatino M, Modanese C, Arnberg L. Depth profile analysis of solar cell silicon by GD-MS. *J Anal At Spectrom*. 2014;29(11):2072-2077.
7. Venzago C, Pisonero J. Chapter 13 glow discharge mass spectrometry. In: *Sector Field Mass Spectrometry for Elemental and Isotopic Analysis*. The Royal Society of Chemistry; 2015:319-380.
8. Di Sabatino M. Detection limits for glow discharge mass spectrometry (GDMS) analyses of impurities in solar cell silicon. *Meas J Int Meas Confed*. 2014;50(1):135-140.
9. Zhang W, Hu Z. Recent advances in sample preparation methods for elemental and isotopic analysis of geological samples. *Spectrochim Acta Part B At Spectrosc*. 2019;160:105690. https://doi.org/10.1016/j.sab.2019.105690
10. Tong SL, Harrison WW. Glow discharge mass spectrometric analysis of non-conducting materials. *Spectrochim Acta Part B At Spectrosc*. 1993;48(10):1237-1245.
11. De Gendt S, Schelles W, Van Grieken R, Müller V. Quantitative analysis of iron-rich and other oxide-based samples by means of glow discharge mass spectrometry. *J Anal At Spectrom*. 1995;10(9):681-687.
12. Betti M. Use of a direct current glow discharge mass spectrometer for the chemical characterization of samples of nuclear concern. *J Anal At Spectrom*. 1996;11(9):855-860.
13. Bogaerts A, Schelles W, Van Grieken R. Analysis of nonconducting materials by dc glow discharge spectrometry. In: *Glow Discharge Plasmas in Analytical Spectroscopy*. John Wiley & Sons, Ltd; 2003:293-315.
14. Milton DMP, Hutton RC. Investigations into the suitability of using a secondary cathode to analyse glass using glow discharge mass spectrometry. *Spectrochim Acta Part B At Spectrosc*. 1993;48(1):39-52.
15. Schelles W, De Gendt S, Muller V, Van Grieken R. Evaluation of secondary cathodes for glow discharge mass spectrometry analysis of different nonconducting sample types. *Appl Spectrosc*. 1995;49(7):939-944.
16. Schelles W, De Gendt S, Maes K, Van Grieken R. The use of a secondary cathode to analyse solid non-conducting samples with direct current glow discharge mass spectrometry: potential and restrictions. *Fresenius J Anal Chem*. 1996;355(7–8):858-860.

17. Schelles W, Van Grieken RE. Direct current glow discharge mass spectrometric analysis of macor ceramic using a secondary cathode. *Anal Chem*. 1996;68(20):3570-3574.
18. Schelles W, Van Grieken R. Quantitative analysis of zirconium oxide by direct current glow discharge mass spectrometry using a secondary cathode. *J Anal At Spectrom*. 1997;12(1):49-52.
19. Qian R, Zhuo S, Wang Z, Robinson PK. Direct current glow discharge mass spectrometric analysis of non-conducting materials using a surface coating method. *J Anal At Spectrom*. 2013;28(7):1061-1067.
20. Barnhart, D., Churchill, G., and Burrows, A., "An exploration of sample preparations and detection limits for conductive, semi-conductive and non-conductive materials as pertaining to the astrum HR-GDMS," in 2nd International Glow Discharge Spectroscopy Symposium, 2014, no. April.
21. Wang, X., Putyera, K., "Full survey chemical analysis of photovoltaic films and interfaces with pulsed fast flow glow discharge mass spectrometry," Application note EAG laboratories, 2020.
22. Paudel G, Kasik M, Di Sabatino M. Investigation of the intensity dependence of glow discharge mass spectrometry quantification on the discharge parameters. *J Anal At Spectrom*. 2019;34(9):1829-1837.
23. Seah MP, Nunney TS. Sputtering yields of compounds using argon ions. *J Phys D Appl Phys*. 2010;43(25):253001. https://doi.org/10.1088/0022-3727/43/25/253001
24. Oechsner H. Sputtering-a review of some recent experimental and theoretical aspects. *Appl Phys*. 1975;8(3):185-198.
25. Seah MP. Pure element sputtering yields using 500–1000 eV argon ions. *Thin Solid Films*. 1981;81(3):279-287.
26. Laegreid N, Wehner GK. Sputtering yields of metals for $ar+$ and $ne+$ ions with energies from 50 to 600 eV. *J Appl Phys*. 1961;32(3):365-369.
27. Schelles W, De Gendt S, Van Grieken RE. Optimization of secondary cathode thickness for direct current glow discharge mass spectrometric analysis of glass. *J Anal At Spectrom*. 1996;11(10):937-941.
28. Vieth W, Huneke JC. Relative sensitivity factors in glow discharge mass spectrometry. *Spectrochim Acta Part B at Spectrosc*. 1991;46(2):137-153.
29. Bogaerts A, Gijbels R. Relative sensitivity factors in glow discharge mass spectrometry: The role of charge transfer ionization. *J Anal At Spectrom*. 1996;11(9):841-847.
30. Bogaerts A, Temelkov KA, Vuchkov NK, Gijbels R. Calculation of rate constants for asymmetric charge transfer, and their effect on relative sensitivity factors in glow discharge mass spectrometry. *Spectrochim Acta Part B at Spectrosc*. 2007;62(4):325-336.
31. Sanderson NE, Hall E, Clark J, Charalambous P, Hall D. Glow discharge mass spectrometry-a powerful technique for the elemental analysis of solids. *Microchim Acta*. Jan. 1987;91(1):275-290.
32. Saito M. Influence of operating parameters on ion intensity in glow discharge mass spectrometry. *Anal Chim Acta*. 1993;274(2):327-334.
33. Tanaka T, Kubota T, Kawaguchi H. Effects of the discharge-gas flow rate on the relative sensitivity factors in glow-discharge mass spectrometry with a grimm-type ion source. *Anal Sci*. 1994;10(6):895-899.
34. Di Sabatino M, Dons AL, Hinrichs J, Arnberg L. Determination of relative sensitivity factors for trace element analysis of solar cell silicon by fast-flow glow discharge mass spectrometry. *Spectrochim Acta - Part B at Spectrosc*. 2011;66(2):144-148.
35. Bogaerts A, Gijbels R. Modeling of glow discharge sources with flat and pin cathodes and implications for mass spectrometric analysis. *J Am Soc Mass Spectrom*. Sep. 1997;8(9):1021-1029.
36. Kasik M, Michellon C, Pitchford LC. Effects of cathode heating in a GDMS system. *J Anal At Spectrom*. 2002;17(10):1398-1399.
37. Rumble J. *CRC Handbook of Chemistry and Physics*. 100thed. CRC Press LLC; 2019.
38. Neauport J, Lamaignere L, Bercegol H, Pilon F, Birolleau J-C. Polishing-induced contamination of fused silica optics and laser induced damage density at 351 nm. *Opt Express*. Dec. 2005;13(25):10163-10171.
39. Li Y, Zheng N, Li H, et al. Morphology and distribution of subsurface damage in optical fused silica parts: bound-abrasive grinding. *Appl Surf Sci*. 2011;257(6):2066-2073.
40. Li Y, Yuan Z, Wang J, Xu Q. Laser-induced damage characteristics in fused silica surface due to mechanical and chemical defects during manufacturing processes. *Opt Laser Technol*. 2017;91:149-158.
41. Wedepohl KH. The composition of the continental crust. *Geochim Cosmochim Acta*. 1995;59(7):1217-1232.
42. Bogaerts, A. and Gijbels, R., "Calculation of crater profiles on a flat cathode in a direct current glow discharge," *Spectrochim Acta - Part B At Spectrosc*, vol. 52, no. 6 PART B, pp. 765–777, 1997.
43. Chapman B. *Glow Discharge Processes: Sputtering and Plasma Etching*. New York: Wiley; 1980.

How to cite this article: Busam J, Stokkan G, Muggerud AMF, Di Sabatino M. Application of 7N In as secondary cathode for the direct current-glow discharge mass spectrometry analysis of solid, fused high-purity quartz. *J Mass Spectrom*. 2021;56(8):e4771. https://doi.org/10.1002/jms.4771